Raman analysis of strain in p-type doped silicon nanostructures

Ferran Ureña-Begara[1], Renaud Vayrette[1], Umesh Kumar Bhaskar[2], Jean-Pierre Raskin[1]

[1]Université catholique de Louvain, Institute of Information and Communication Technologies, Electronics and Applied Mathematics (ICTEAM), Louvain-la-Neuve, Belgium

[2]Purdue University, School of Electrical and Computer Engineering, West Lafayette, USA

***** Corresponding author: ferran.urena@uclouvain.be

Keywords:

Raman, Young's modulus, strain, stress, doping.

Abstract:

In this work, 100 nm-thick boron-doped silicon beams with doping levels between $1{\cdot}10^{16}$ and $1{\cdot}10^{20}$ cm^{-3} undergoing uniaxial tensile strain are investigated by Raman spectroscopy. The structures exhibit a noticeable reduction in Young's modulus (~20%) compared with the value reported for bulk. The traditional Raman shift coefficients used to determine stress and strain in bulk structures are revised and appropriate corrections are implemented to account for the observed changes in Young's modulus. Interestingly, the Raman shift-strain relation in silicon nanostructures with strain along the [110] direction is found to be independent of size effects and doping. In contrast, the Raman shift-stress relation is found to be highly dependent on size effects. The dependency of the Fano line-shape parameters, used to fit the Raman first order peak in structures with high levels of doping, with strain is also reported. The results are shown to be crucial

to accurately determine stress and strain from Raman measurements in doped silicon nanostructures and devices with size effects.

I. INTRODUCTION

Strained silicon is commonly used in the microelectronic industry to fabricate high-speed CMOS devices and in the fabrication of micro- and nano-electromechanical systems (MEMS and NEMS), e.g. strained-channels in metal-oxide-semiconductor field-effect transistors (MOSFETs) and pressure and force sensors [1-3]. In these devices, a precise knowledge of the values of stress and strain is vital for a proper device operation.

In order to characterize strain, Raman spectroscopy is a widely used technique due to its non-destructive nature. It can readily achieve a spatial resolution below 1 μm and it does not require sample preparation [4]. The technique measures the difference in energy between the incident photons of a laser beam and the photons originated from the inelastic scattering with the lattice vibrations of the sample (phonons). In unstressed pure silicon, the first order Raman peak can be fitted with a symmetrical Lorentzian line-shape with a central frequency ~520 cm^{-1} [4]. It is known however, that in the presence of high levels of doping ($\eta > 1 \cdot 10^{18}$ cm^{-3}), the line-shape of the first order peak becomes asymmetric and it is not possible to accurately fit it with a symmetrical Lorentzian function [5]. In addition, in the presence of stress, the frequency of the first order Raman peak shifts towards lower (tensile stress) or higher (compressive stress) wavenumbers. Stress and strain are linearly related to the shift in Raman frequency and can be determined if the corresponding strain- and stress-shift coefficients are known [4]. These coefficients depend upon several material constants including the elastic compliance coefficients and the phonon deformation potentials (PDPs) [4].

The elastic coefficients and the PDPs have been reported to vary with size and with the level of doping [6-8]. The onset of the dimensions at which size effects are observed is still under debate although the general agreement is that size effects are mainly observed at the nanoscale when surface effects are non-negligible [9]. Nevertheless, despite that the impact of size and doping on the silicon material constants has been largely discussed, the Raman stress- and strain-shift coefficients in structures with size effects and high levels of doping have not received much attention. This is important since nowadays devices are well into the nanometer regime and high levels of doping are commonly used in the semiconductor industry. Thus, a proper extraction of the stress and strain in these devices is vital.

In this work, we use a microelectromechanical system (MEMS) concept to characterize stress and strain in an array of 100 nm-thick silicon free-standing beams with different lengths and doping concentrations. The use of different geometries has allowed us to investigate the size effects and the impact of doping in a wide range of structures under different values of strain and stress. Three different levels of doping (boron) were investigated, $1{\cdot}10^{16}$, $1{\cdot}10^{17}$, and $1{\cdot}10^{20}$ cm^{-3}. The levels of doping were verified from resistivity measurements obtained by the 4-point probes method. Scanning electron microscopy (SEM) measurements were used to precisely determine the elongation of the beams and thus obtain accurate values of strain. From the SEM measurements, the strain, stress and Young's modulus were determined and compared with previous reported values. Finally, Raman measurements were performed in all the structures to determine the impact of doping and the strain- and stress shift coefficients.

The paper is organized as follows. Section II describes the fabrication details and the methodology used to determine strain and stress from the structures. Section III is devoted to the main results. Strain and stress measurements as well as the Young's moduli determined of all the structures are presented. Raman measurements of the structures with strain and doping are described followed

by a thorough analysis of the impact of doping on the structures. The section ends with the determination of the Raman shift-strain and -stress coefficients. The main conclusions are finally drawn in Section IV.

II. METHODOLOGY

Fig. 1a, shows a schematic of the structures used in this work to characterize stress and strain. Each structure consists of a silicon nitride (Si_3N_4) actuator and an attached silicon beam. The structures were fabricated starting with a silicon-on-insulator (SOI) wafer with a top silicon layer t∼100 nm and aligned along the [110] direction. After patterning the silicon beams on the top silicon layer, a silicon nitride layer is deposited at 800 °C and patterned to make the actuators. Finally, the structures are released by etching away the SiO_2 sacrificial layer with hydrofluoric acid (HF). After the release of the structures and due to the high deposition temperature of the silicon nitride, the actuator contracts at room temperature and induces a tensile strain in the attached silicon beams. The magnitude of the induced strain depends on the length of the actuator.

In order to determine the induced strain, a pair of cursors is fabricated alongside the actuators (Fig. 1a). Strain is determined right after the release of the beams by measuring the displacement of the attached cursors with SEM. Also, in addition to the structures shown in Fig. 1a, 'U' shaped silicon beams with four aluminum contacts at the ends were fabricated to determine the resistivity by the 4-probe contact method. Fig. 1b shows a microscope image of one of these samples with two of the aluminum pads used for the probes contact at the ends. More detailed information about the test concept, fabrication and resistivity measurements can be found elsewhere [10-12].

After the release of the structures, the induced strain is determined from the SEM measurements of the cursors displacement by:

$$\varepsilon = \ln\left(\frac{L_0 + u}{L_0}\right) \quad (1)$$

Here L_0 and u are the initial length and the cursors displacement of the silicon beams, respectively. The stress applied by the actuator on the silicon beams is also determined from the cursor displacements and the known geometry dimensions of the structures also verified by SEM:

$$\sigma = E_A \frac{S_A}{S}\left(\varepsilon_A^{mis} - \frac{u}{L_0}\right) \quad (2)$$

Here S_A, E_A and ε_A^{mis} are the cross-section, Young's modulus and mismatch strain of the actuator, respectively, and S the cross-section of the silicon beams. The mismatch strain is that applied by a free actuator, i.e. with no attached silicon beam, and the Young's modulus of the actuator is experimentally determined by nanoindentation ~235 GPa [10].

In order to evaluate the impact of doping on the Young's modulus of the samples and the Raman shift-strain and -stress relation, Raman measurements were performed using a LabRam HR 800 confocal system with a high numerical aperture lens (N.A. = 0.9). A 458 nm wavelength laser working in backscattering configuration and with a penetration depth in silicon of ~300 nm was selected [4]. The penetration depth of this laser assures that the entire silicon thickness of the beams is probed while minimizes the signal coming from the silicon substrate (this facilitates the deconvolution process of the two signals).

III. RESULTS AND DISCUSSION

A. Stress and strain determination

After the determination of stress and strain using Eqs. 1 and 2, the Young's modulus is obtained from the slope of a linear regression fitting of the stress-strain values of each beam length. Fig. 2 shows the stress-strain relation and the Young's modulus determined for the samples with the three levels of doping investigated.

The Young's modulus of the structures varies between 130 – 139 GPa. These values represent a reduction of ~20% compared with the Young's modulus reported for bulk silicon along the [110] direction (169 GPa, black solid line in Fig. 2) [13]. Young's modulus values smaller than those reported for bulk silicon have been found previously in works with silicon nanostructures and are generally attributed to the reduced dimensions of the structures [14]. At small dimensions, the surface-to-volume ratio increases, and surface effects including surface stress and native oxide cannot be neglected. In these structures, the surface effects may significantly affect the material properties and the measured values may largely differ compared with the corresponding values in bulk [15]. The values reported in Fig. 2 thus, correspond to the effective Young's modulus (E_{eff}) of the structures.

The onset at which size effects become relevant is still under debate. In a previous work of our group, the Young's modulus of a series of 200 nm-thick undoped silicon beams was determined using the same test concept reported above (Fig. 1) [9]. The average value compiled from a set of ~100 samples with varying geometries was 165 ± 5 GPa and it was concluded that size effects had a negligible impact on the Young's modulus in structures with dimensions down to 200 nm. In the present work however, the observed reduction in Young's modulus might be also affected by the medium-high doping levels used with the structures and as a consequence, the silicon crystalline structure of the beams may have resulted altered or damaged. Previous works reporting on the dependence of the elastic properties in silicon with doping concluded however, that the elastic constants were not significantly affected even at high levels of doping ($\eta \sim 1 \cdot 10^{20}$ cm^{-3}) [6, 7]. Furthermore, it has been reported that in order to observe a significant change in the elastic constants of silicon, amorphization must take place, e.g. by using very high energies during the implantation process [16]. This has been confirmed by the work of Ng *et al*. [6] in samples with a boron concentration of $\sim 1.7 \cdot 10^{20}$ cm^{-3}. In these samples, the Young's modulus determined for the

[110] direction is ∼163 GPa [6]. This value represents a reduction ∼6 GPa compared with the value typically reported for the Young's modulus in bulk silicon (169 GPa) and is in perfect agreement with the small differences in Young's modulus observed between the medium and the heavily doped samples in this work (∼9 GPa) (Fig. 2).

B. Raman measurements and doping analysis

Fig. 3 shows the Raman spectra obtained for the unstressed samples and for the three levels of doping. In the absence of strain the Raman spectrum of monocrystalline silicon consists of a main peak centered at ∼520.7 cm^{-1} and can be fitted with a symmetrical Lorentzian function and a FWHM (full width at half maximum) ∼3.1 ± 0.1 cm^{-1} [4]. Amorphicity and, in general, damages in the crystal lattice of silicon are factors which are known to alter the shape (symmetry) and increase the FWHM [17]. As observed with the $1{\cdot}10^{16}$ and $1{\cdot}10^{17}$ cm^{-3} doped samples (Fig. 3), the first order peak is perfectly fitted with a single symmetrical Lorentzian function centered at ∼520.7 cm^{-1} and a FWHM ∼3 cm^{-1}. These values thus, confirm that the crystalline structure of the beams has not been compromised (due to the implantation process) and that the large reduction observed in the Young's modulus, ∼20%, is indeed due to size effects.

For the heavily doped structures ($\eta \sim 1{\cdot}10^{20}$ cm^{-3}) however, the first order peak in the absence of strain cannot be fitted with a symmetrical Lorentzian line-shape (dashed line in Fig. 3). Also, as shown in Fig. 3, the FWHM of this function should be ∼ 6 cm^{-1} in order to obtain a reasonable good fitting. This asymmetry and increase in the FWHM of the first order peak has been largely studied and is commonly observed in heavily doped samples ($\eta > 1{\cdot}10^{18}$ cm^{-3}) [5]. In these samples, the asymmetry of the peak arises as a result of the interaction between the discrete energies of the optical phonons with those of the continuum of electronic scattering due to the large density of free carriers (Fano effect) [18]. As a result of the Fano effect, the frequency, FWHM and shape of the first order Raman peak might be significantly altered compared with the typical values reported for

undoped silicon. In the presence of the Fano effect, the shape of the first order Raman peak can be fitted using a modified Lorentzian function to account for the asymmetry of the peak:

$$I = A\frac{(q+\epsilon)^2}{1+\epsilon^2} \tag{3}$$

with $$\epsilon = \frac{\omega - \omega_0}{\Gamma} \tag{4}$$

Here A is a constant related to the intensity of the peak, q is an asymmetry factor and Γ is a factor related to the line-width of the peak [5]. ω and ω_0 are the Raman frequency and the reference Raman frequency in bulk undoped silicon, respectively. As it can be seen in Fig. 3, the fitting of the Raman spectrum of the heavily doped samples (solid line) with both, a Fano component (Eqs. 3 and 4) and a Lorentzian component (to account for the signal coming from the silicon substrate), is excellent and confirms that the asymmetry and increase of the FWHM of these samples arises from the Fano interaction.

Cerdeira *et al*. [19] reported on the relation between the parameters q and Γ with the wavelength. Whereas the asymmetry parameter q was found to depend on the incident wavelength, Γ was found to be wavelength independent. For a 458 nm wavelength and a $1.6\cdot10^{20}$ cm^{-3} p-type doped sample, the reported values for the parameters q and Γ were 7.0 and 8.24 cm^{-1}, respectively. Fig. 4 shows the relation obtained in this work for these parameters and for the 458 nm radiation. As it can be seen, in the absence of stress, the values determined for the $1\cdot10^{20}$ cm^{-3} doped beams are 7.3 and 5.7, respectively. Both values are in close agreement with those determined by Cerdeira *et al*. [19] for the $1.6\cdot10^{20}$ cm^{-3} doping concentration, although the value of Γ slightly differs most likely due to differences in doping concentration used in both studies ($1\cdot10^{20}$ and $1.6\cdot10^{20}$ cm^{-3}). A quantitative analysis of the dependency of q and Γ with strain is challenging due to the complex structure of the silicon energy bands and their dependency with strain [5]. The task becomes more aggravated with the current samples where the presence of surface effects results in an intricate material structure

and composition whose analysis is beyond the scope of this work. However, from a qualitative point of view, some conclusions can be drawn. Thus, as observed in Fig. 4, the asymmetry parameter q^{-1} decreases with increasing stress. This is because the continuum of energies due to electronic scattering shifts with stress and at sufficient values of stress it does not longer overlap with that of the phonon scattering [5]. Likewise, the parameter Γ, related to the half-width at half maximum of the peak, decreases with increasing stress and at high levels of stress tends to approximate that of the symmetrical Lorentzian peak observed in bulk silicon (FWHM ~3.1 cm^{-1}).

C. Raman shift-strain and -stress relation

Fig. 5 shows the evolution of the Raman spectra of the samples with strain. As it can be seen, the first order Raman peak shifts towards lower wavenumbers with increasing tensile strain. At large values of strain, the component due to silicon of the substrate is also visible. Different from the peak due to the silicon of the beams, this component does not shift with strain and can be fitted with a symmetrical Lorentzian function centered at 520.7 cm^{-1}. The shift in frequency of the peak from the silicon beams is linear with the applied stress and strain through the Raman shift-strain and -stress coefficients, respectively [4].

Fig. 6a shows the linear relation between the Raman shift and the applied strain and the Raman shift -strain coefficients extracted from the slope of the least-squares linear regression for each level of doping investigated. Surprisingly, despite the significant decrease in Young's modulus observed in the present structures, the Raman shift-strain coefficient in all cases does not vary compared with that reported for bulk silicon along the [110] direction (b=-343) [20]. In contrast however, the Raman shift-stress relation (Fig. 6b) along the [110] direction is:

$$\Delta\omega\ (cm^{-1}) = -2.54\ \sigma\ (\mathrm{GPa}) \qquad (5)$$

Compared with the commonly used expression to determine stress in bulk silicon, $\Delta\omega\ (cm^{-1}) = -2\ \sigma\ (\mathrm{GPa})$ [4], the Raman shift-stress coefficient determined in Eq. 5, has experienced a variation ~30 %. This is a significant variation and implies that in those materials where surface effects cannot be neglected, e.g. thin-film materials, stress determination using the Raman shift-stress relation intended for bulk materials may lead to severe errors. The relation between the Raman shift-stress 'a' and -strain 'b' coefficients is given by:

$$a = b/E_{eff} \tag{6}$$

Eq. 6 thus, allows the determination of the Raman shift-stress coefficient once the effective Young's modulus of the sample is known.

IV. CONCLUSIONS

In conclusion, the impact of doping and size effects on silicon nanostructures has been investigated by Raman spectroscopy. The results show that the Young's modulus of the nanostructures drastically changes mainly due to size effects (effective Young's modulus). For the structures with $1{\cdot}10^{16}$ and $1{\cdot}10^{17}$ cm^{-3} doping levels, the Raman analysis does not show any significant difference due to the doping and compared with that typically reported for bulk structures. However, for the $1{\cdot}10^{20}$ cm^{-3} doping level, the full-width at half-maximum, and the asymmetry of the peak experienced some significant changes due to the Fano effect. For these structures, the relation between the asymmetry parameter q and Γ (related to the line-width of the peak) with stress were also determined. The values were shown to be in close agreement with those previously reported for bulk doped silicon. Likewise, despite the drastic changes in Young's modulus, the Raman shift-strain coefficient determined in the nanostructures does not show any significant change compared with previous values reported for bulk silicon. In contrast, however, the commonly used linear relation between the Raman shift and stress to characterize stress in bulk silicon underwent a large

variation ~30%. Based on the measurements of strain and stress, a new Raman shift-stress coefficient to calculate stress from the Raman shift was derived. The results of this work should be useful in the determination of stress and strain from Raman measurements in nanostructures with medium and large levels of doping.

References

[1] D. Ramos, E. Gil-Santos, O. Malvar, J. M. Llorens, V. Pini, A. San Paulo, M. Calleja, and J. Tamayo, "Silicon nanowires: where mechanics and optics meet at the nanoscale," *Scientific reports*, vol. 3, p. 3445, 2013.

[2] M. L. Lee, E. A. Fitzgerald, M. T. Bulsara, M. T. Currie, and A. Lochtefeld, "Strained Si, SiGe, and Ge channels for high-mobility metal-oxide-semiconductor field-effect transistors," *Journal of Applied Physics*, vol. 97, no. 1, p. 1, 2005.

[3] Y. Cui, Q. Wei, H. Park, and C. M. Lieber, "Nanowire nanosensors for highly sensitive and selective detection of biological and chemical species," *Science*, vol. 293, no. 5533, pp. 1289–1292, 2001.

[4] I. De Wolf, H. Maes, and S. K. Jones, "Stress measurements in silicon devices through raman spectroscopy: bridging the gap between theory and experiment," *Journal of Applied Physics*, vol. 79, no. 9, pp. 7148–7156, 1996.

[5] F. Cerdeira, T. Fjeldly, and M. Cardona, "Effect of free carriers on zone-center vibrational modes in heavily doped p-type Si. ii. optical modes," *Physical Review B*, vol. 8, no. 10, p. 4734, 1973.

[6] E. J. Ng, V. A. Hong, Y. Yang, C. H. Ahn, C. L. Everhart, and T. W. Kenny, "Temperature dependence of the elastic constants of doped silicon," *Journal of microelectromechanical systems*, vol. 24, no. 3, pp. 730–741, 2015.

[7] Z. Zeng, X. Ma, J. Chen, Y. Zeng, D. Yang, and Y. Liu, "Effects of heavy phosphorus-doping on mechanical properties of czochralski silicon," *Journal of Applied Physics*, vol. 107, no. 12, p. 123503, 2010.

[8] M. Chandrasekhar, H. Chandrasekhar, M. Grimsditch, and M. Cardona, "Study of the localized vibrations of boron in heavily doped Si," *Physical Review B*, vol. 22, no. 10, p. 4825, 1980.

[9] F. Ureña, S. H. Olsen, L. Šiller, U. Bhaskar, T. Pardoen, and J.-P. Raskin, "Strain in silicon nanowire beams," *Journal of Applied Physics*, vol. 112, no. 11, p. 114506, 2012.

[10] S. Gravier, M. Coulombier, A. Safi, N. André, A. Boé, J.-P. Raskin, and T. Pardoen, "New on-chip nanomechanical testing laboratory-applications to aluminum and polysilicon thin films," *Journal of microelectromechanical systems*, vol. 18, no. 3, pp. 555–569, 2009.

[11] U. Bhaskar, V. Passi, S. Houri, E. Escobedo-Cousin, S. H. Olsen, T. Pardoen, and J.-P. Raskin, "On-chip tensile testing of nanoscale silicon free-standing beams," *Journal of Materials Research*, vol. 27, no. 3, pp. 571–579, 2012.

[12] R. Vayrette, J.-P. Raskin, and T. Pardoen, "On-chip fracture testing of freestanding nanoscale materials," *Engineering Fracture Mechanics*, vol. 150, pp. 222–238, 2015.

[13] M. A. Hopcroft, W. D. Nix, and T. W. Kenny, "What is the young's modulus of silicon?" *Journal of microelectromechanical systems*, vol. 19, no. 2, pp. 229–238, 2010.

[14] H. Sadeghian, C. Yang, J. Goosen, E. Van Der Drift, A. Bossche, P. French, and F. Van Keulen, "Characterizing size-dependent effective elastic modulus of silicon nanocantilevers using electrostatic pull-in instability," *Applied Physics Letters*, vol. 94, no. 22, p. 221903, 2009.

[15] H. Sadeghian, H. Goosen, A. Bossche, B. Thijsse, and F. Van Keulen, "On the size-dependent elasticity of silicon nanocantilevers: impact of defects," *Journal of Physics D: Applied Physics*, vol. 44, no. 7, p. 072001, 2011.

[16] R. Bhadra, J. Pearson, P. Okamoto, L. Rehn, and M. Grimsditch, "Elastic properties of si during amorphization," *Physical Review B*, vol. 38, no. 17, p. 12656, 1988.

[17] I. De Wolf, C. Jian, and W. M. van Spengen, "The investigation of microsystems using raman spectroscopy," *Optics and Lasers in Engineering*, vol. 36, no. 2, pp. 213–223, 2001.

[18] U. Fano, "Effects of configuration interaction on intensities and phase shifts," *Physical Review*, vol. 124, no. 6, p. 1866, 1961.

[19] F. Cerdeira, T. A. Fjeldly, and M. Cardona, "Interaction between electronic and vibronic raman scattering in heavily doped silicon," *Solid State Communications*, vol. 13, no. 3, pp. 325–328, 1973.

[20] F. Ureña, S. Olsen, and J.-P. Raskin, "Raman measurements of uniaxial strain in silicon nanostructures," *Journal of Applied Physics*, vol. 114, no. 14, 2013.

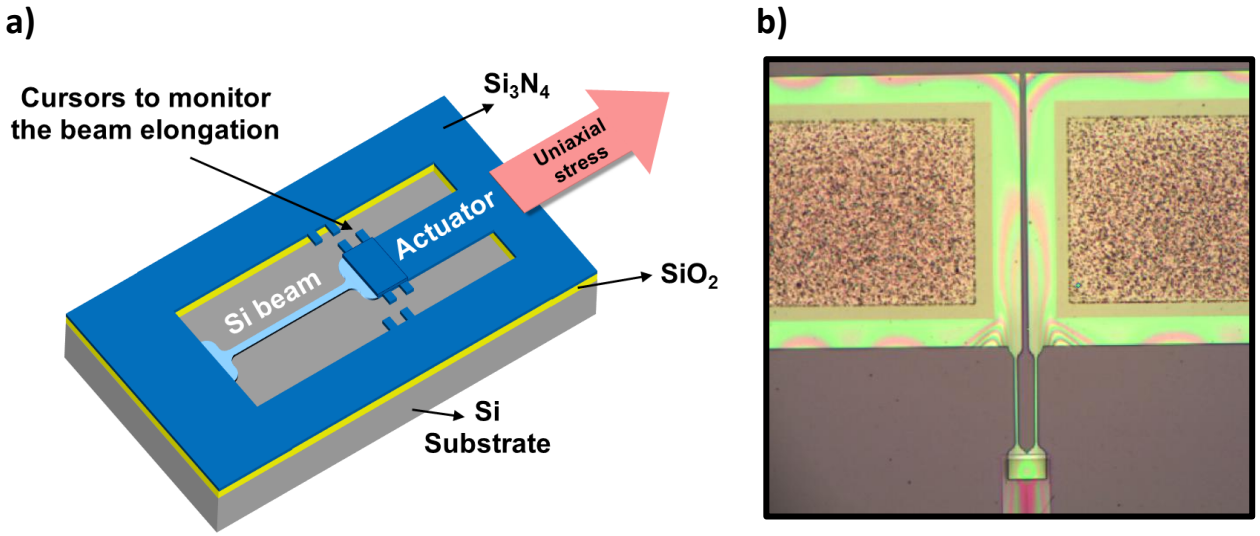

Fig. 1 a) Schematic of the MEMS structures used in this work to characterize stress and strain. b) Microscope image of a 'U' shaped structure used for resistivity measurements.

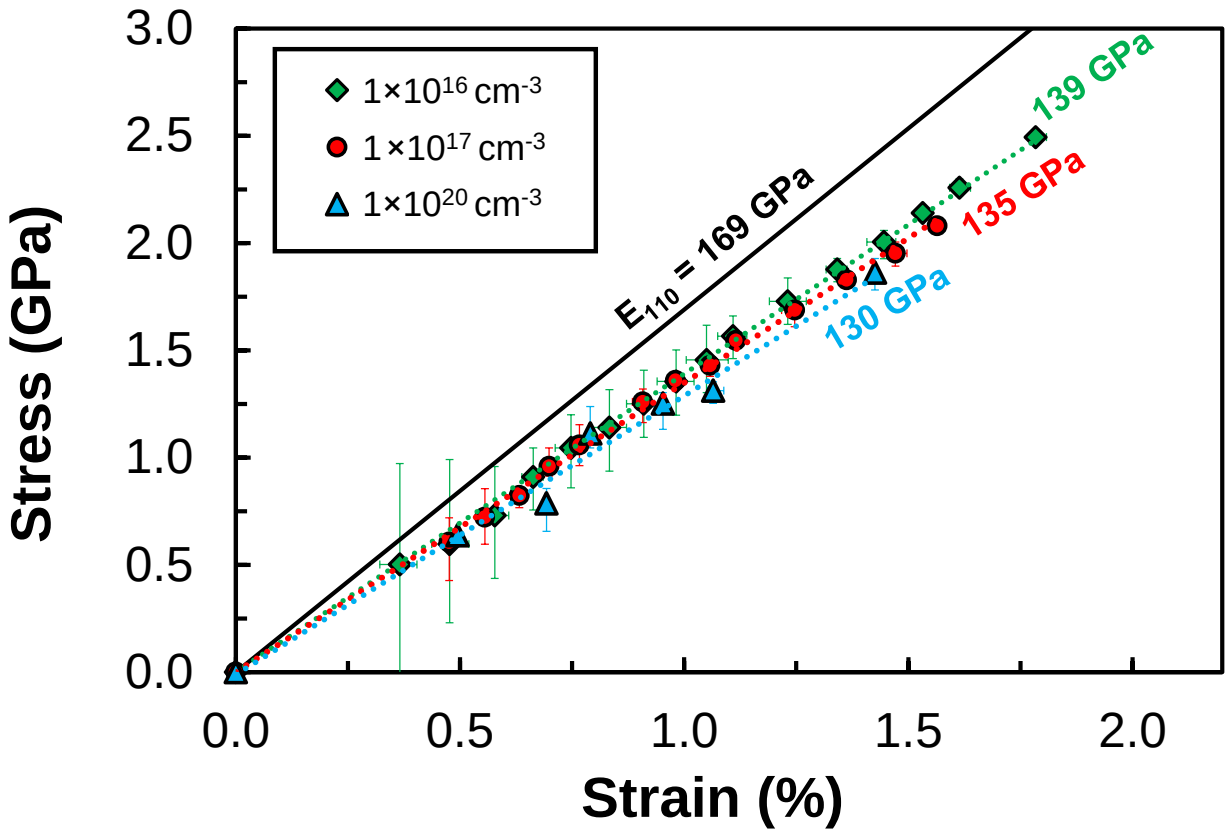

Fig. 2 Stress-strain relation and effective Young's modulus extracted for the three doping levels used in the work.

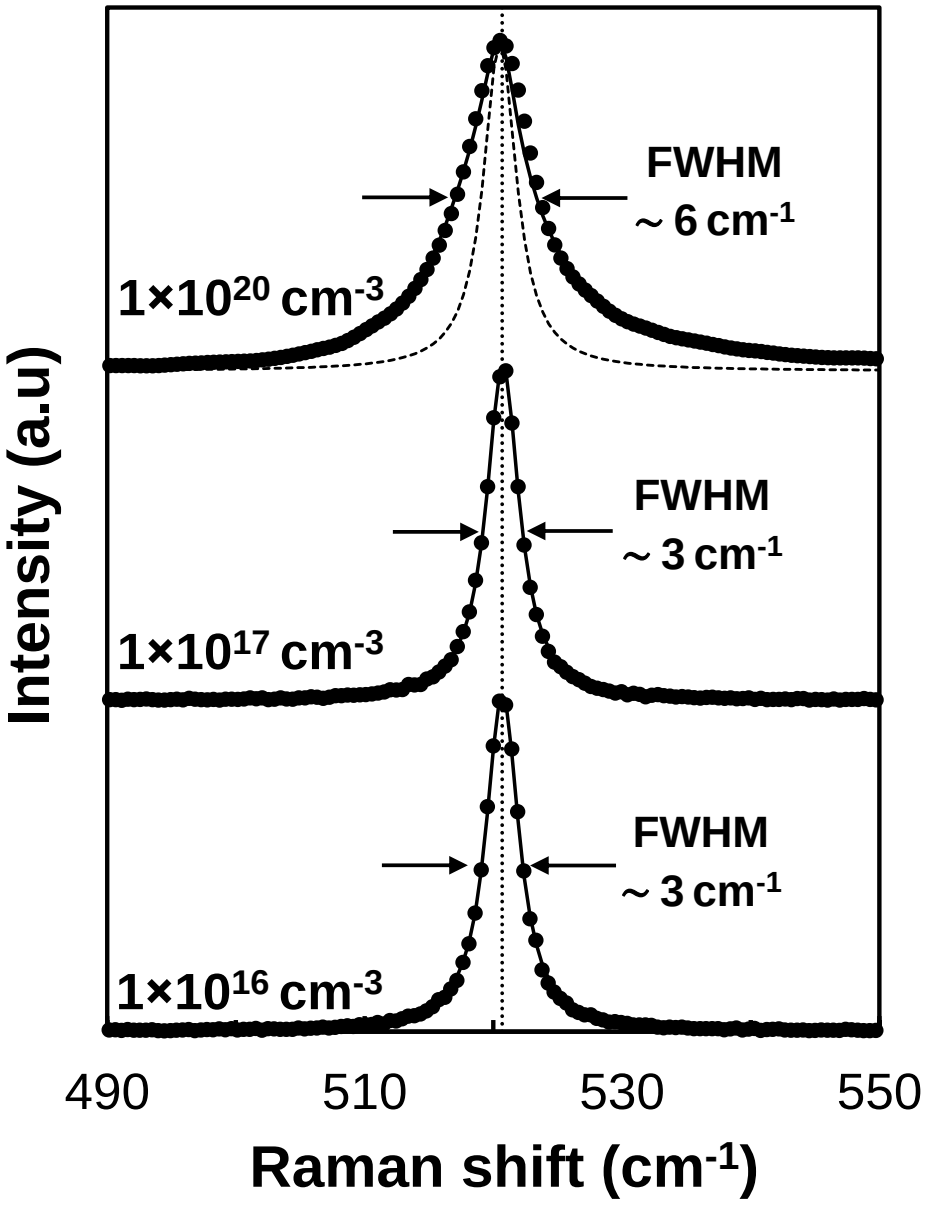

Fig. 3 First order Raman peak of the unstressed samples. The samples with $1{\cdot}10^{16}$ and $1{\cdot}10^{17}$ cm^{-3} levels of doping are perfectly fitted with a single symmetrical Lorentzian function (solid lines). However, the sample with $1{\cdot}10^{20}$ cm^{-3} doping level, requires a Lorentzian and a Fano component to obtain a good fitting.

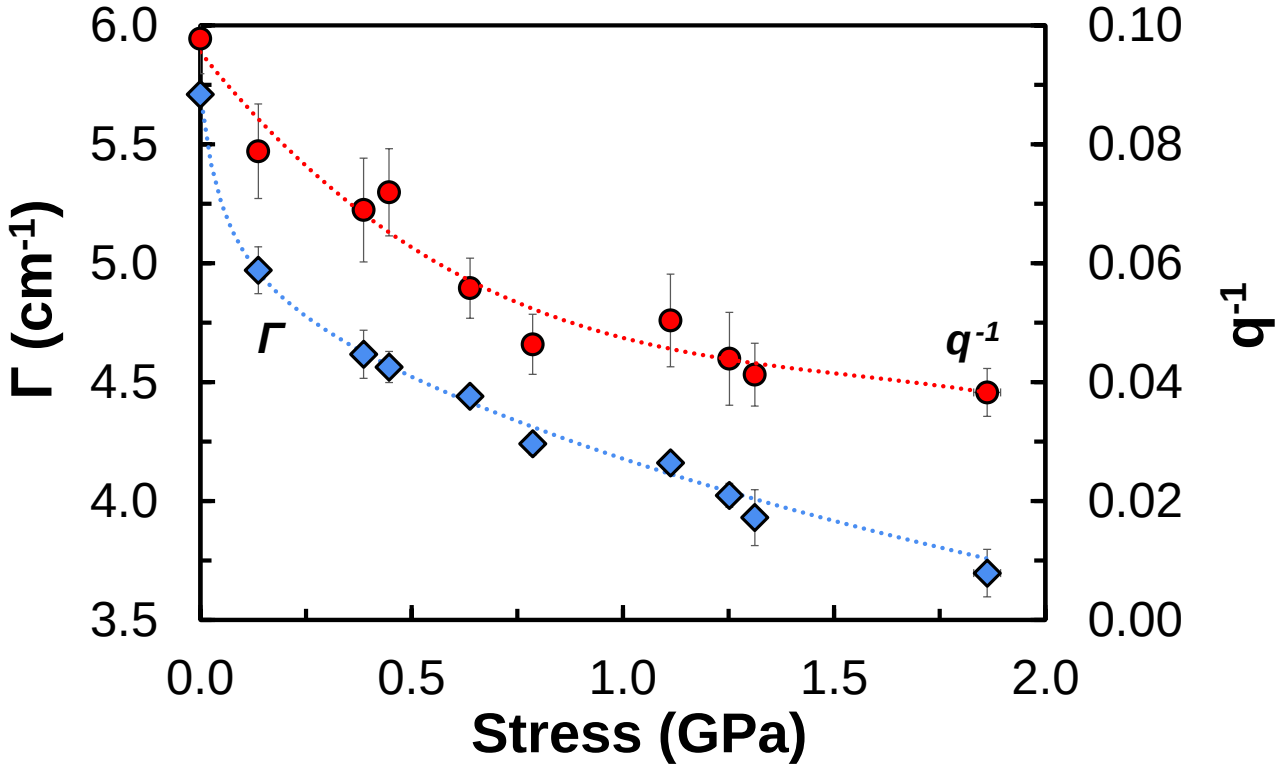

Fig. 4 Relation between the asymmetry parameter q^{-1} and Γ with stress for the $1 \cdot 10^{20}$ cm^{-3} doped structures. Dotted lines are only a guide to the eye.

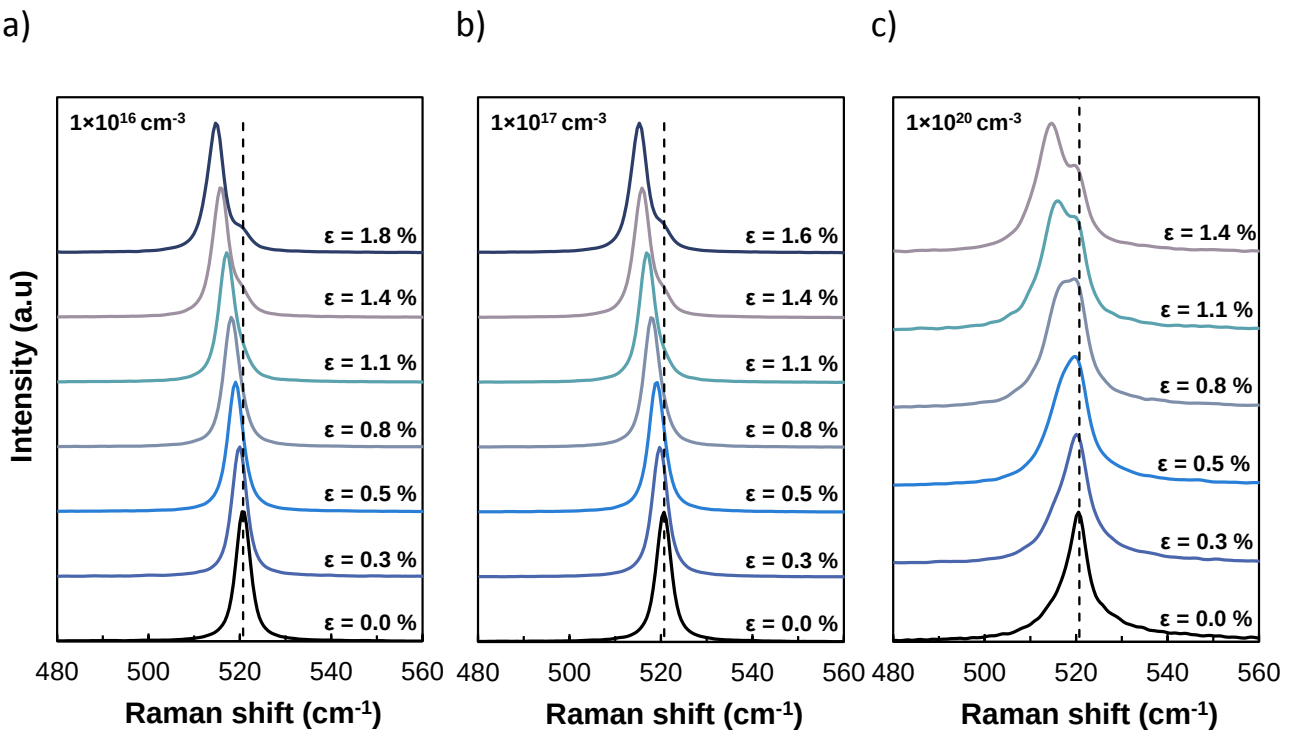

Fig. 5 Evolution of the Raman spectra with strain for the three levels of doping used in the work. a) $1 \cdot 10^{16}$ cm^{-3}, b) $1 \cdot 10^{17}$ cm^{-3} and c) $1 \cdot 10^{20}$ cm^{-3}

a)

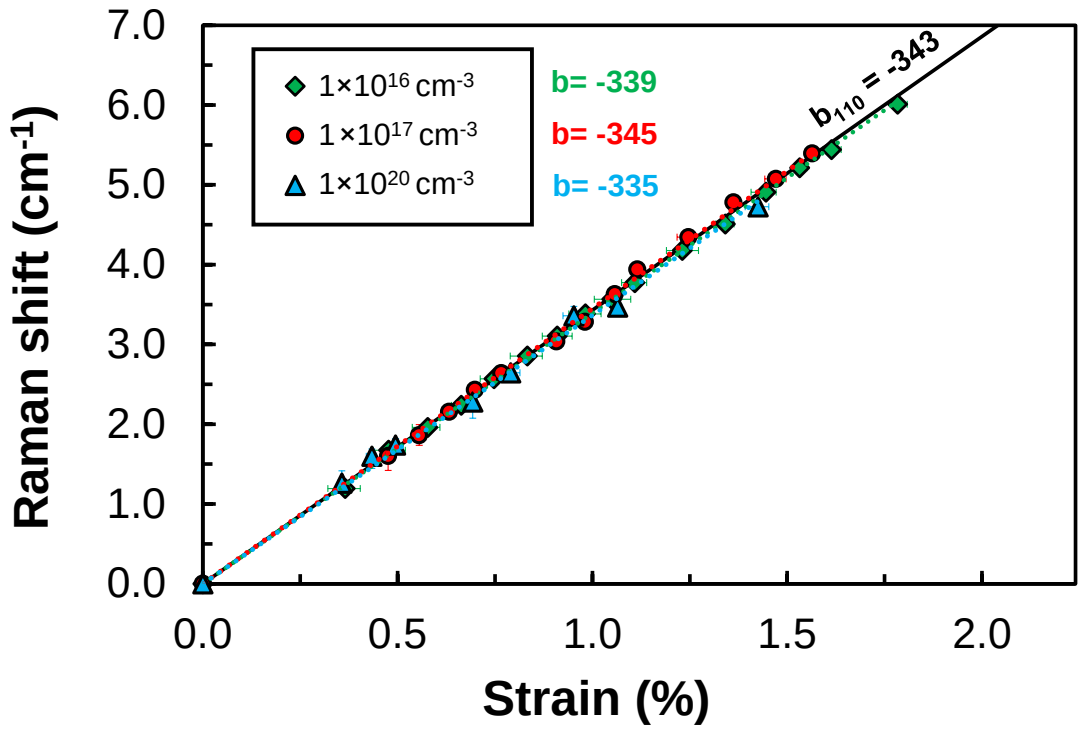

b)

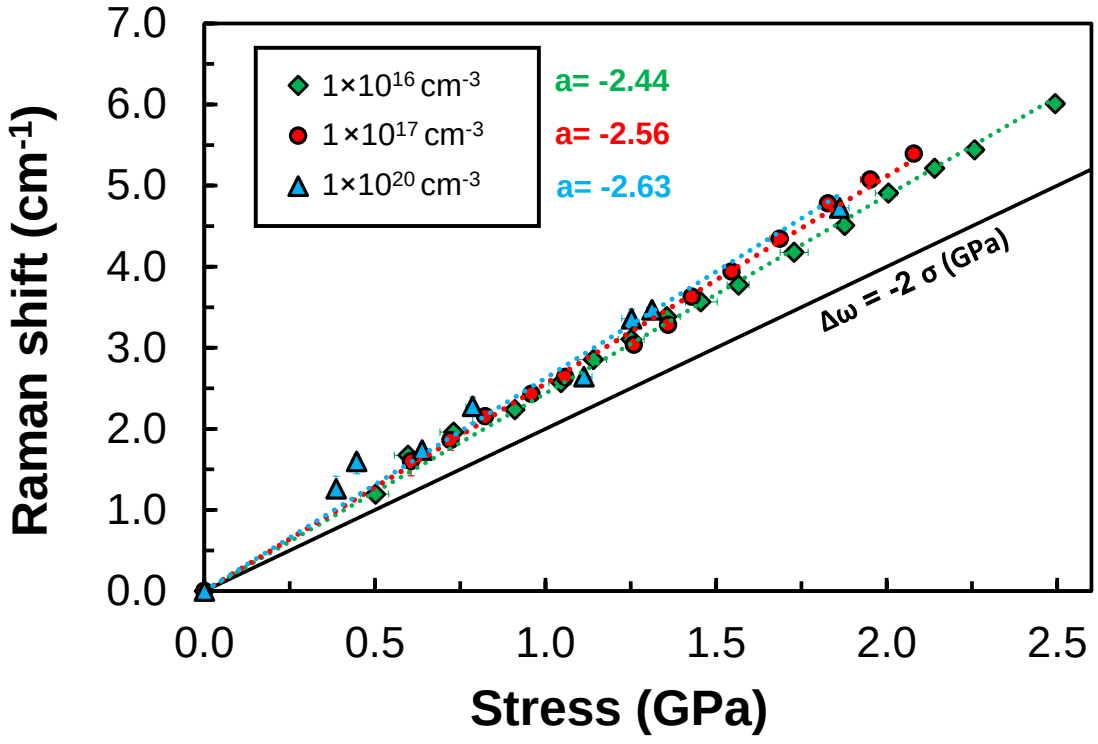

Fig. 6 Raman shift-strain (a) and -stress (b) relations for the three doping concentrations used in the work.